

Lee-Yang edge singularities in QCD via the Dyson-Schwinger Equations

Zi-Yan Wan¹, Yi Lu¹, Fei Gao^{2a}, and Yu-xin Liu^{13b}

¹ Department of Physics and State Key Laboratory of Nuclear Physics and Technology, Peking University, Beijing 100871, China

² School of Physics, Beijing Institute of Technology, 100081 Beijing, China

³ Center for High Energy Physics, Peking University, Beijing 100871, China

August 20, 2024

Abstract. We take the Dyson-Schwinger Equation approach of QCD for the quark propagator at complex chemical potential to study the QCD phase transition. The phase transition line of the (2+1)-flavor QCD matter in the imaginary chemical potential region is computed via a simplified truncation scheme, whose curvature is found to be consistent with the one at real chemical potential. Moreover, the computation in the complex chemical potential plane allows us to determine the location of the Lee-Yang edge singularities. We show explicitly that the critical end point coincides with the Lee-Yang edge singularities on the real μ_B axis. We also investigate the scaling behavior of the singularities and discuss the possibility of extrapolating the CEP from a certain range of chemical potential.

PACS. XX.XX.XX No PACS code given

1 Introduction

Many efforts have been made both experimentally and theoretically to explore the phase structure of QCD in the plane of temperature and chemical potential [1, 2, 3, 4, 5, 6, 7, 8, 9, 10]. At vanishing chemical potential, lattice QCD simulation has made great progresses and predicted a crossover at about $T = 156.5$ MeV [11, 12]. However, due to the sign problem, it is difficult for lattice QCD to approach large chemical potential region. In particular, the up to date computation from functional QCD approaches [13, 14, 15, 16] and also effective theories [2, 17] have converging estimations that the the critical end point (CEP) of chiral phase transition is located at a large chemical potential, $\mu_B \approx 600$ MeV. Therefore, people appeal to the imaginary chemical potential where there is no sign problem and can offer more information about the phase structure and CEP.

It has been known that the imaginary chemical potential offers a way of extracting the curvature of the phase transition line of QCD after assuming the line is continuous from imaginary to real chemical potential. And the analytical structure of the thermodynamic quantities determines the phase structure. In detail, the edge singularities, i.e. the Lee-Yang zeroes, are located in the complex plane of the chemical potential and at second or first order phase transition, the singularities reach the real axis [18, 19].

Consequently, the Lee-Yang zeroes also determine the convergence radius of the expansion for finite chemical potential applied in lattice QCD simulations [20, 21, 22]. Moreover, there are more interesting features in the imaginary chemical potential region. For instance, there exists the Roberge-Weiss phase transition, which can be connected to the confinement due to its relation with $Z(N_c)$ symmetry [23, 24]. The imaginary chemical potential dependence of chiral condensate, i.e. the dual condensate [25, 26], is thus also related to the confinement.

Plenty of novel phenomena rise up in the complex chemical potential region of QCD. However, the related physics have not yet been fully investigated theoretically under the QCD approaches. In particular, the Dyson-Schwinger equations (DSEs) approach has been shown successful of incorporating both the dynamical chiral symmetry breaking (DCSB) and the confinement physics of non-perturbative QCD [7, 27, 28], which is also well developed for the application on exploring the QCD phase structure in recent years [13, 14, 15]. We then present for the first time a DSEs study on the Lee-Yang edge (LYE) singularities and its trajectory on the complex μ_B plane. Most importantly, we show directly the close relation between the LYE singularities and the CEP location.

In specific, we provide both an estimation of the CEP location, as well as a direct computation of the trajectory of the LYE singularities. We provide an estimate of the critical region by studying the extrapolation of the trajectory towards the actual CEP location. Our studies

^a Corresponding author: fei.gao@bit.edu.cn

^b yxliu@pku.edu.cn

of the scaling behavior of LYE singularities give a clear picture on the QCD phase structure, with connections to various different aspects such as the critical scaling, the Columbia plot, the convergence radius of the equation of state, etc. In particular, We illustrate that the trajectory of LYE singularities satisfies the CEP scaling in a large range of temperature. We then show that the LYE singularities offers a new way of estimating the location of CEP, and our estimation is close to the onset regime of CEP at $T \simeq 110$ MeV and $\mu_B \simeq 600$ MeV obtained from extracted information from LYE singularities in combination with the current best truncation schemes of functional QCD approaches.

The remainder of this paper is organised as follows. In Sec. 2, we present the framework of Dyson-Schwinger equations we implemented here. In Sec. 3, we deliver the results of Lee-Yang edge singularities, and in Sec. 4 we make some detailed analysis for the QCD phase structure based on the Lee-Yang edge singularities. In Sec. 5, we analyse the dependence of the result on the parameters in the truncation scheme. In Sec. 6, we briefly summarize the main results and make some discussions.

2 The DSEs approach and the truncation scheme

In this paper, we take the DSEs approach to study the QCD phase structure at finite temperature T and chemical potential μ_B . Our main focus is to solve the quark DSE, schematically shown in Fig. 1. At finite temperature T and quark chemical potential μ , the $O(4)$ symmetry of the momentum p is broken to $O(3)$ (\vec{p}, ω_n), where $\omega_n = 2\pi T(2n+1)$ is the Matsubara frequency for fermion. The dressed quark propagator is written as:

$$[S(p)]^{-1} = i\tilde{\omega}_n \gamma_4 C(\vec{p}, \tilde{\omega}_n) + i\vec{p}\vec{\gamma} A(\vec{p}, \tilde{\omega}_n) + B(\vec{p}, \tilde{\omega}_n), \quad (1)$$

with abbreviation $\tilde{\omega}_n = \omega_n + i\mu$, A, B, C are scalar functions that need to be determined. Together with the dressed gluon propagator $D_{\mu\nu}$ and the gluon-quark interaction vertex Γ_μ , Fig. 1 can be expressed as:

$$[S(p)]^{-1} = [S_0(p)]^{-1} + \Sigma(p),$$

$$\Sigma(p) = C_F Z_1 g^2 T \sum_n \int \frac{d^3 \vec{q}}{(2\pi)^3} \gamma_\mu S(q) \Gamma_\nu(p, q; k) D_{\mu\nu}(k), \quad (2)$$

with the renormalized bare quark propagator

$$[S_0(p)]^{-1} = Z_2 i\not{p} + Z_2 Z_m m_f, \quad (3)$$



Fig. 1. A schematic plot for the quark DSE. The line with black dot stands for the bare quark propagator, and the line with solid blobs stand for the full propagators and the circle for the interaction vertex.

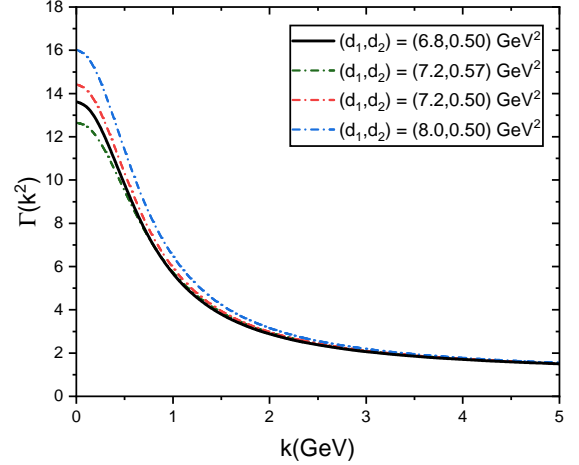


Fig. 2. The running behaviour of the quark-gluon vertex function $\Gamma(k^2)$ in the truncation scheme Eq. (5). A comparison of the function under different choices of the parameter (d_1, d_2) is also shown, including the choice taken from Ref. [29] as $(6.8, 0.5)$ GeV² (solid black curve) and for other values (colored dash-dotted curves, to be investigated in Sec. 5).

where Z_2, Z_1, Z_m are quark wave function, vertex, and quark mass renormalization constants, and $C_F = \frac{N_c^2 - 1}{2N_c}$ is the expectation value of the Casimir operator $\hat{C}_{2, SU(N_c)}$; $g^2 = 4\pi\alpha(\zeta)$ is the coupling constant which is dependent on the renormalization point ζ . The renormalisation condition of the quark DSE is:

$$Z_2 = 1 - \Sigma_d(\zeta^2), \quad Z_2 Z_m = 1 - \frac{\Sigma_s(\zeta^2)}{m_f}, \quad (4)$$

with $\Sigma(p^2) \equiv i\not{p}\Sigma_d(p^2) + \Sigma_s(p^2)$.

We solve the quark DSE with a renormalization point at $\zeta = 40$ GeV, with the corresponding running coupling taken as $\alpha(\zeta) = 0.1286$, and the average current mass of u, d quark $m_l = (m_u + m_d)/2 = 2.09$ MeV.

For the truncation of the quark-gluon interaction vertex, we follow the Ansätze used in Refs. [14, 29], which follows from the Slavnov Taylor identity (STI) with a parametrised form for the non-Abelian part of the vertex Γ as:

$$\Gamma_\mu(p, q; k) = \gamma_\mu \cdot \Gamma(k^2) \cdot \left(\delta_{\mu,4} \frac{C(p) + C(q)}{2} + \delta_{\mu,i} \frac{A(p) + A(q)}{2} \right),$$

$$\Gamma(k^2) = \frac{d_1}{d_2 + k^2} + \frac{k^2}{\Lambda^2 + k^2} \left(\frac{\beta_0 \alpha(\zeta) \ln[k^2/\Lambda^2 + 1]}{4\pi} \right)^{2\delta}. \quad (5)$$

where the anomalous dimension $\beta_0 = (11N_c - 2N_f)/3$, $\delta = -9N_c/(44N_c - 8N_f)$. For the parameters we will first follow Ref. [29] (set B_{2+1}) to take $\alpha(\zeta) = 0.3$, $\Lambda = 1.4$ GeV, $d_1 = 6.8$ GeV² and $d_2 = 0.5$ GeV², which are determined by solving the Bethe-Salpeter equation for the 2+1-flavor case. The running behavior of such a $\Gamma(k^2)$ is shown as the solid black curve in Fig. 2. Moreover, we also

show the dependence of d_1 and d_2 on $\Gamma(k^2)$ by varying the value of the two parameters, which is also shown in Fig. 2. A more detailed analysis on the parameter dependence for d_1 and d_2 will be given in Sec. 5.

The (2+1)-flavor gluon propagator takes the input from the called “functional-lattice” gluon propagator in Ref. [30]. In the vacuum, the Landau gauge gluon propagator $D_{\mu\nu}$ is expressed as:

$$D_{\mu\nu}(p) = D(p)P_{\mu\nu}, \quad \text{with } P_{\mu\nu} = \delta_{\mu\nu} - \frac{p_\mu p_\nu}{p^2}, \quad (6)$$

and $D(p)$ the gluon dressing function, which includes both the lattice results at small momentum and the FRG results at large momentum:

$$D(p) = \frac{(a^2 + p^2) / (b^2 + p^2)}{M^2(p^2) + p^2 [1 + c \ln(d^2 p^2 + e^2 M^2(p^2))]^\gamma}, \quad (7)$$

with $M^2(p) = \frac{f^4}{g^2 + p^2}$,

where the anomalous dimension $\gamma = \frac{13-4/3N_f}{22-4/3N_f}$, along with the other parameters given by $\{a, b, c, d, e\} = \{1 \text{ GeV}, 0.735 \text{ GeV}, 0.12, 0.0257 \text{ GeV}^{-1}, 0.081 \text{ GeV}^{-1}\}$, together with $\{f, g\} = \{0.65 \text{ GeV}, 0.87 \text{ GeV}\}$.

At finite temperature T and baryon chemical potential μ_B , the gluon propagator is split into the longitudinal (L) and transversal (T) part with respect to the heat bath by the corresponding projectors $P_{\mu\nu}^{T,L}$.

$$\begin{aligned} P_{\mu\nu}^T &= (1 - \delta_{\mu 4})(1 - \delta_{\nu 4})P_{\mu\nu}, \\ P_{\mu\nu}^L &= P_{\mu\nu} - P_{\mu\nu}^T, \end{aligned} \quad (8)$$

Also, the finite T and μ_B effect on the gluon propagator is incorporated into the longitudinal part D^L by the thermal mass, which can be taken as that provided by the one-loop hard thermal loop (HTL) calculations [31, 32]:

$$D_{\mu\nu} = D^T(\Omega_{nm}^2, \vec{k})P_{\mu\nu}^T + D^L(\Omega_{nm}^2 + m_g^2, \vec{k})P_{\mu\nu}^L. \quad (9)$$

$$m_g^2 = \frac{g^2}{3} \left[(N_c + \frac{N_f}{2})T^2 + \frac{3N_f}{2\pi^2}\mu^2 \right]. \quad (10)$$

with $\mu = \mu_B/3$, i.e. the 3-flavor degenerate case. As for the case of a complex chemical potential with $\text{Im } \mu = \phi\pi T$ satisfying $\phi \in [-1, 1]$, the thermal mass m_g^2 is extended to complex plane according to the analytical continuation of Eq. (10). In practice, due to the small effect of $\text{Im } \mu$ on the gluon sector, we maintain only the real part of m_g^2 for convenience.

First, we solve the quark DSE in Eq. (2) self-consistently in the vacuum, and obtain the quark mass function $M(p) = B(p)/A(p)$ as shown in Fig. 3. which is consistent with the results from the lattice QCD simulation [33] and the fRG-DSE calculation [30]. Moreover, we focus on the quark condensate $\langle \bar{\psi}\psi \rangle$ which can be calculated from the quark propagator:

$$\langle \bar{\psi}\psi \rangle = Z_2 Z_m N_c T \sum_n \int \frac{d^3 \vec{p}}{(2\pi)^3} \text{tr}[S(\tilde{\omega}_n, \vec{p})], \quad (11)$$

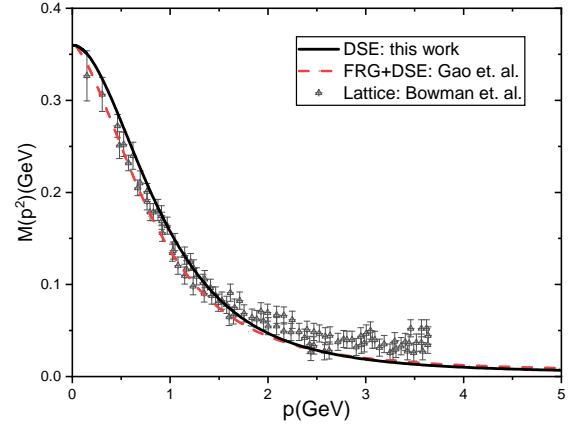


Fig. 3. Calculated quark mass function in the vacuum, and the comparison with the lattice QCD result [33] and the fully coupled functional QCD result [30].

For a non-zero bare quark mass m_l , Eq. (11) will be linearly divergent. Here, one of the regularization scheme is that eliminates the divergent part via the derivative form as done in Refs. [30, 34]:

$$\langle \bar{\psi}\psi \rangle_{\text{reg}} = \langle \bar{\psi}\psi \rangle - m \frac{\partial}{\partial m} \langle \bar{\psi}\psi \rangle. \quad (12)$$

Another choice is the reduced condensate, defined from the strange quark condensate in Refs. [29, 35]

$$\langle \bar{\psi}\psi \rangle_{\text{red}} = \langle \bar{\psi}\psi \rangle^l - \frac{m_l}{m_s} \langle \bar{\psi}\psi \rangle^s, \quad (13)$$

with $m_s = 27 m_l = 56.43 \text{ MeV}$. With the quark propagator determined by solving Eq. (2), we obtained the regularized condensate from Eq. (12) as $\langle \bar{\psi}\psi \rangle_{\text{reg}} = (333.6 \text{ MeV})^3$, and the reduced condensate from Eq. (13) as $(335.8 \text{ MeV})^3$. The obtained regularized quark condensate satisfies excellently the Gell-Mann-Oakes-Renner Relation:

$$f_\pi^2 m_\pi^2 = 2m^\zeta \langle \bar{\psi}\psi \rangle_\zeta, \quad (14)$$

with the vacuum pion decay constant $f_\pi = 89 \text{ MeV}$ and the pion mass $m_\pi = 139 \text{ MeV}$.

At finite temperature and chemical potential, one can make use of the maximum of the light-quark chiral susceptibility χ_m^l to determine the pseudo-critical temperatures, which is defined from the chiral condensate as

$$\chi_m^l = \frac{\partial \langle \bar{\psi}\psi \rangle_{\text{reg}}}{\partial m_l}, \quad (15)$$

For the reduced condensate in Eq. (13), the expression of χ_m can be reduced to $\partial \langle \bar{\psi}\psi \rangle^l / \partial m_l$ due to the small variations on the strange condensate according to m_l . Based on this, we take a further approximation of Eq. (15) as:

$$\chi = \frac{\partial B_0}{\partial m_l}, \quad (16)$$

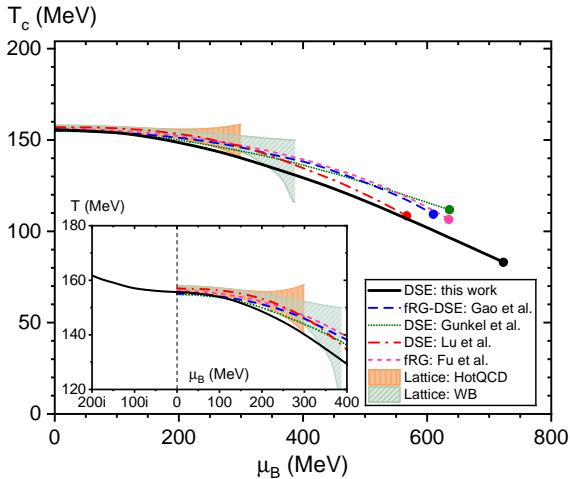


Fig. 4. The obtained phase diagram of the chiral phase transition identified with the susceptibility Eq. (15), compared with the lattice QCD [11, 12] and other functional QCD [13, 14, 16, 35] results. The solid dots denote the positions of the CEP. A comparison between pure imaginary and real μ_B is also shown in the sub-figure.

where B_0 is the value of B at the first Matsubara frequency and zero three-momentum $B(\tilde{\omega}_0, \mathbf{0})$. Such an approximation has been confirmed to be efficient in, e.g., Ref. [34], with only a few MeV difference of the extracted pseudo-critical temperatures. Then we obtain the phase transition line as displayed in Fig. 4.

At zero chemical potential, our obtained pseudo-critical temperature is $T_c = 155.7 \text{ MeV}$, which agrees excellently with the up-to-date lattice QCD results [11, 12] and the functional QCD results [13, 14, 16, 29, 35]. At larger chemical potential and lower temperature, the chiral susceptibility as a function of T and μ becomes sharper and sharper, and the critical temperature decreases. Such a quantitative nature is embedded in the curvature of the phase transition line:

$$\frac{T_c(\mu_B)}{T_c(0)} = 1 - \kappa_2^B \left(\frac{\mu_B}{T_c(0)} \right)^2 + \kappa_4^B \left(\frac{\mu_B}{T_c(0)} \right)^4 + \dots \quad (17)$$

The curvature κ_2^B is extracted from a region of $\mu_B \in (0, 360) \text{ MeV}$ with a result $\kappa_2^B = 0.026$. We also check for the pure imaginary chemical potential in a range of $\mu_B^2 \in (-210^2, 0) \text{ MeV}^2$, and obtain the corresponding curvature $\kappa_2^B = 0.024$. The phase transition line at real and pure imaginary μ_B is also displayed together in Fig. 4, which shows that the continuity is valid at zero μ_B , in agreement with what is found in Ref. [36]. Eventually, the susceptibility is divergent at the location of CEP, which is found at $(T_{CEP}, \mu_{B,CEP}) = (83 \text{ MeV}, 723 \text{ MeV})$. Compared with a similar truncation scheme as in Ref. [29], one can notice that the T_{CEP} is almost the same, but the $\mu_{B,CEP}$ is larger due to a different treatment on the gluon sector.

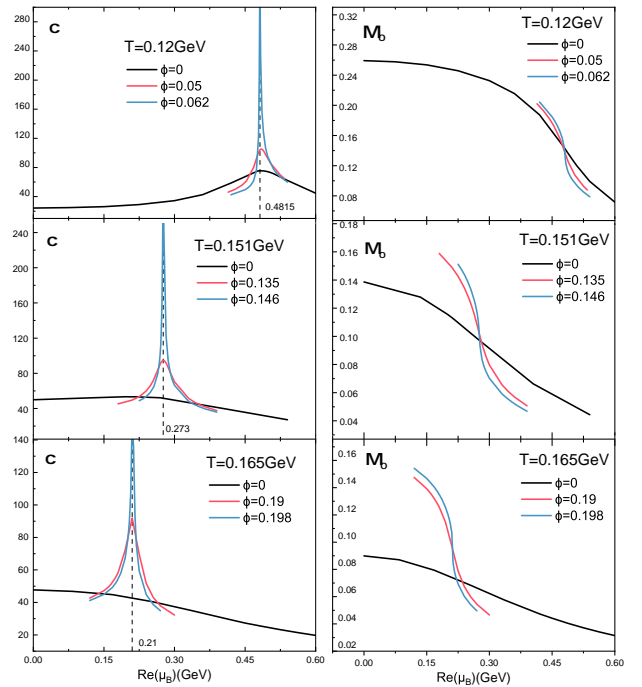


Fig. 5. The obtained complex chemical potential dependence of chiral susceptibility χ in Eq. (16) (left panels) and the mass M_0 (right panels) at temperatures $T = 120 \text{ MeV}$ (the first row), $T = 151 \text{ MeV}$ (the second row), $T = 165 \text{ MeV}$ (the third row). The singularities which are marked by the dashed vertical lines correspond to the critical chemical potentials.

3 The Lee Yang edge singularities

In Refs. [18, 19], Lee and Yang have revealed the relation between the phase transition and zeroes of the partition functions Z on the complex plane of the μ : the Lee-Yang Zeroes. These zeroes form branch cuts on the μ plane, and the edge branch points are known as the Lee-Yang edge (LYE) singularities. In short, when the LYE singularities reach the μ real axis, the singularities correspond to the critical end point. While the branch cut crosses the real axis, the first order phase transition occurs. These can be well understood due to the properties of pressure $P = \frac{1}{V} T \ln Z$ around the Lee-Yang Zeroes. Briefly speaking, the first derivative of P is discontinuous crossing the branch cut, and continuous but non-analytical at the LYE singularities. This suggests that the same criterion, i.e. the susceptibility χ in Eq. (15) for the phase transition line introduced in Sec. 2 can also be applied to determine the location of LYE singularities, when the chemical potential is extended to the complex values.

In specific, we scan the χ over the T - $\text{Re } \mu$ plane at a given imaginary chemical potential $\text{Im } \mu = \phi \pi T$ for $\phi \in (0, 1)$, and the obtained result is illustrated in Fig. 5. It can be seen that when $T > T_{CEP}$, there exist apparent singularities on the complex μ plane. For example, at $T = 120 \text{ MeV}$, the susceptibility χ is continuous along $\text{Re}(\mu)$ at $\phi = 0$. As ϕ approaches the critical value $\phi_c = 0.062$, M_0 becomes steeper with a sharper peak of χ and finally

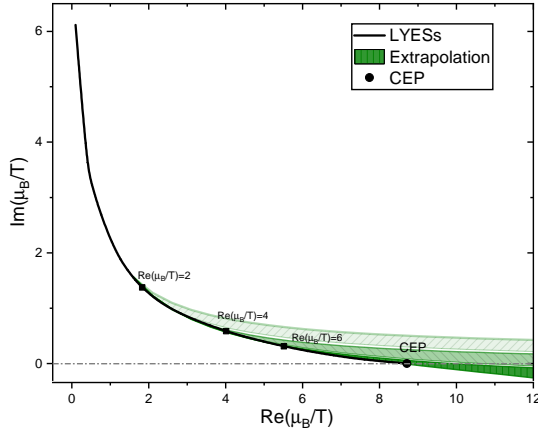


Fig. 6. The obtained trajectory of the LYE singularities on the $\text{Re}(\mu_B/T) - \text{Im}(\mu_B/T)$ plane, together with the CEP which is marked on the $\text{Im}(\mu_B/T) = 0$ axis. The extrapolation analysis of the trajectory using data within $\text{Re}(\mu_B/T) \in (0, 2)$, $(0, 4)$ and $(0, 6)$ are also shown with the error estimates, which are displayed as the light, medium and dark colored bands, respectively.

reaches the singularity at $\text{Re} \mu_{LYE} = 481.5 \text{ MeV}$. For a higher temperature, e.g. $T = 150 \text{ MeV}$, one can observe a similar behavior of χ . Also, at $T > T_c$ the singularity still exists in the complex μ_B plane. The edge of such a singularity μ_{LYE} is scanned in a wide range of temperature to yield a trajectory of the LYE singularities, the obtained results are displayed in Fig. 6. Our result shows apparently that the trajectory crosses the real axis of μ_B exactly at $T = T_{CEP}$, which implies a strong connection between the QCD critical end point and the LYE singularities.

We then provide an estimate on the critical region of the CEP via an extrapolation study of the obtained μ_{LYE} data. In specific, we consider the data within several small chemical potential regions and carry out the extrapolation with the convergent Padé polynomials (in $N = nm$, $n \in [1, 2]$, $m \in [n, 3]$) towards a higher $\text{Re} \mu_B$ to compare with the calculated trajectory and also the CEP position. The regions we take are $\text{Re}(\mu_B/T) \in [0, 2]$, $[0, 4]$ and $[0, 6]$ and the corresponding analyses are shown in Fig. 6. It is found that the quality of the extrapolation becomes better with an extending range of $\text{Re}(\mu_B/T)$ being included. Within $\text{Re}(\mu_B/T) \in [0, 2]$ where the lattice extrapolation approach is still controllable, the extrapolated position of the CEP has a systematic error of more than 30%. It is also estimated that a knowledge of $\text{Re}(\mu_B/T)$ with the range corresponds to $\Delta T = |T/T_{CEP} - 1| \sim 20\%$ and $\Delta \mu = |\mu/\mu_{B,CEP} - 1| \sim 15\%$, is required in order to get an error control of 10% for the extrapolated CEP. In short, additional information at large $\text{Re} \mu_B$ is still required in order to provide a precise determination of the CEP position.

4 Analysing the trajectory of the LYE singularities

In the vicinity of the LYE singularities where the second-order phase transition occurs, the correlation length tends to be divergent, and the critical behavior is only determined by the symmetry and dimension of the system which can be classified into various universality classes. Then one can describe the critical behavior including the location of LYE singularities of a specific system by universal quantities and the non-universal relevant thermodynamic parameters. For the Ising model and $O(N)$ model, expressed by the scaling field z , the singularities locate at $z = t/h^{1/\beta\delta} = |z_c|e^{i\pi/2\beta\delta}$ [37, 38], where t and h are the general scaling variables with t being the reduced temperature, and h being the symmetry breaking field. The $|z_c|$, β and δ are universal scaling parameters which can be determined in the universality class analysis, and some of which are listed in Table 1.

In the chiral limit, the QCD Lagrangian has $SU_R(2) \times SU_L(2) \cong O(4)$ symmetry. Therefore, for a small quark mass, the critical behavior is expected to be described by the 3D $O(4)$ universality class. According to Refs. [43, 44], the thermodynamic parameters T , μ_B and with the light-to-strange quark mass ratio m_l/m_s can be mapped onto the scaling variables t and h at zero chemical potential as:

$$t = t_0^{-1} \left[\frac{T - T_c^0}{T_c^0} + \kappa_2^B \left(\frac{\mu_B}{T_c^0} \right)^2 \right], \quad (18)$$

$$h = h_0^{-1} \frac{m_l}{m_s},$$

from which one can derive the expression for the location of the singularities at specific temperature [44]:

$$(\mu_{LYE})^2 = \frac{(T_c^0)^2}{\kappa_2^B} \left[\frac{|z_c|}{z_0} e^{i\pi/2\beta\delta} \left(\frac{m_l}{m_s} \right)^{\frac{1}{\beta\delta}} - \frac{T - T_c^0}{T_c^0} \right], \quad (19)$$

where κ_2^B is the curvature of the phase transition line and T_c^0 the phase transition temperature at zero chemical potential in chiral limit. In turn, the singularity corresponds to the convergence radius of the expansion with respect to the chemical potential. As determined in the last section, we have $\kappa_2^B = 0.026$ and $m_l/m_s = 1/27$. The remaining parameters are T_c^0 and z_0 , the former of which can be interpreted as the critical temperature in the chiral limit. With our truncation scheme in Eq. (5), such critical temperature is found at $T_c^0 = 0.138 \text{ GeV}$. Also, the scale

Table 1. The critical exponents β , δ and the location of Lee Yang Edge Singularities $|z_c|$ for different universality classes [39, 40, 41, 42].

	β	δ	$ z_c $
3d $Z(2)$	0.33	4.79	2.43
3d $O(4)$	0.38	4.82	1.69
Mean field	0.5	3	1.89

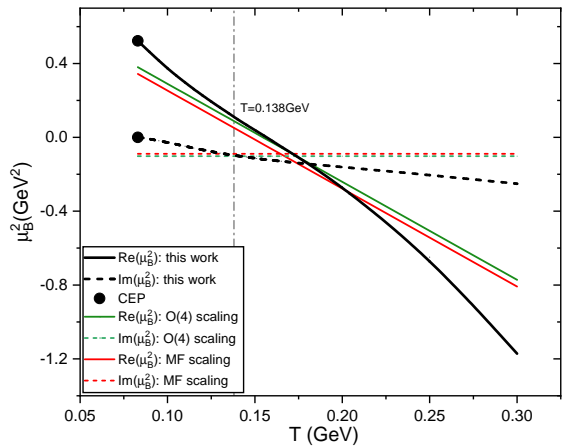


Fig. 7. The obtained temperature dependence of the squared complex chemical potential of the LYE singularity μ_{LYE}^2 , including its real part (solid line) and imaginary part (dashed line), respectively. The dashed vertical line is at $T_c^0 = 138$ MeV. The case of CEP is also marked with the black solid dots.

factor expected to be $z_0 \in (1, 2)$ [44] and here we simply take $z_0 = 1.5$.

On the other hand, the quark gap equation under the current truncation scheme is expected to be in the mean field universality class. To investigate this, we take Eq. (19) to explore the scaling behavior of the singularities. In specific, we study the temperature dependence of μ_{LYE}^2 for both its real and the imaginary part, which is shown explicitly in Fig. 7. For the real part of μ_{LYE}^2 , the T dependence is approximately linear, as expected in Eq. (19). However, the T dependence of $\text{Im}\mu_{LYE}^2$ is not negligible, not only close to the CEP but also at $T = T_c^0 = 0.138$ GeV. This suggests an additional temperature dependence of the z_c and thus a deviation of the scaling behavior to either the 3D $O(N)$ or the mean field universality class, for a physical quark mass.

Finally, consider the region near the CEP, the universality class is expected to be $Z(2)$ symmetry. By performing the linear mapping of the thermodynamic parameters (T, μ_B) to the scaling variables (t, h) :

$$\begin{pmatrix} t \\ h \end{pmatrix} = \mathbb{M} \begin{pmatrix} T - T_{CEP} \\ \mu_B - \mu_{B,CEP} \end{pmatrix}, \quad \mathbb{M} = \begin{pmatrix} t_T & t_\mu \\ h_T & h_\mu \end{pmatrix}, \quad (20)$$

one can derive the $Z(2)$ scaling formula of the LYE singularities [37, 48]:

$$\begin{aligned} \mu_{LYE} &\sim \mu_{B,CEP} - c_1(T - T_{CEP}) + ic_2(T - T_{CEP})^{\beta\delta}, \\ \text{with } c_1 &= \frac{h_T}{h_\mu}, \quad c_2 = x_{LY} \frac{t_\mu^{\beta\delta}}{h_\mu} \left(\frac{t_T}{t_\mu} - \frac{h_T}{h_\mu} \right)^{\beta\delta}. \end{aligned} \quad (21)$$

where x_{LY} is the imaginary part of LYE singularity in Ising model and reads $x_{LY} = |z_c|^{-\beta\delta}$.

By analysing the scaling behavior of the imaginary part of the chemical potential with respect to the reduced temperature as shown in Fig. 8, the critical region

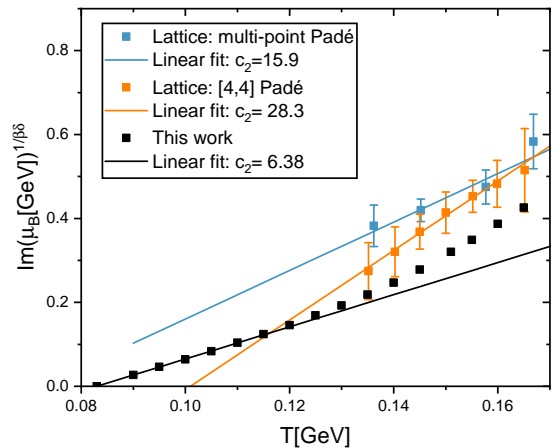


Fig. 8. The scaling behavior of the imaginary part of the chemical potential and a linear fit of $\text{Im}[\mu_B]^{1/(\beta\delta)}$ and T together with the LYE singularities from lattice simulations [45, 46, 47]. The parameter c_2 can be directly extracted from the slope, and applied to estimate the CEP location. Generally speaking, for larger c_2 , one typically gets a higher temperature for CEP.

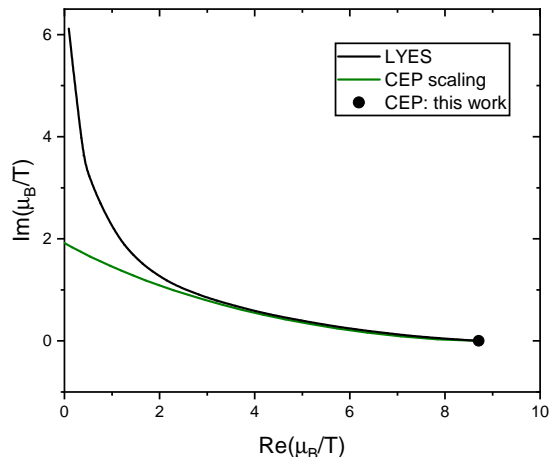


Fig. 9. The LYE singularities trajectory (black), which is well compared with the extracted CEP scaling trajectory (green) from Eq. (21).

can be determined as $\ln((T - T_{CEP})/T_{CEP}) < -1$, i.e. $T \in [83, 110]$ MeV. Also, we perform a linear fit between the calculated $\ln|\text{Im}\mu_{LYE}|$ and $\ln|T - T_{CEP}|$ in the vicinity of CEP to extract the critical exponents $\beta\delta$. This yields $\beta\delta = 1.38$, which slightly differs from the exact value of $Z(2)$ universality class shown in Table 1 due to the lack of detailed critical information in current truncation scheme. However, the CEP scaling behavior is clear and the constants c_1 and c_2 in Eq. (21) can be estimated by fitting with our results within the critical region. The corresponding CEP scaling trajectory is obtained and extrapolated towards small $\text{Re}\mu_B$, shown as the green line in Fig. 9, which shows that the CEP scaling extrapolation is consistent with the calculated trajectory near CEP.

Our results show that the Z(2) scaling works well for the LYE singularities, and therefore, one may directly apply the Ising parameterization to study the CEP. Firstly, we apply the following parameterization as it can well describe the equation of state of QCD [49, 50, 51]. Typically, we take the form as shown in Ref. [49]:

$$\begin{aligned} \frac{\mu_B - \mu_{B,CEP}}{\mu_{B,CEP}} &= -t\omega\rho \cos \alpha_1 - h\omega \cos \alpha_2, \\ \frac{T - T_{CEP}}{T_{CEP}} &= f_{PT}(t) + h\omega \sin \alpha_2, \end{aligned} \quad (22)$$

with $\omega = 1$, $\rho = 2$, $\alpha_1 = \tan^{-1}(2\kappa\mu_{B,CEP}/T_c(0))$ and $\alpha_2 = \alpha_1 + \pi/2$ in our case. The mapping function f_{PT} is calibrated so that at $h = 0$, Eqs. (22) becomes exactly the parametric equations of the phase transition line in Eq. (17), which requires

$$f_{PT}(t) = \frac{\mu_{B,CEP}}{2T_{CEP}} (2 - t\omega\rho \cos \alpha_1) t\omega\rho \sin \alpha_1. \quad (23)$$

This gives then immediately the dimensionless slope parameter \bar{c}_2 as:

$$\bar{c}_2 = x_{LY} \frac{\left(\frac{T_{CEP}}{\mu_{B,CEP}}\right)^{\beta\delta} \omega \sin \alpha_1}{(\omega\rho \sin \alpha_1)^{\beta\delta}} \left(\frac{T_{CEP}}{\mu_{B,CEP}} \cot^2 \alpha_1 + 1 \right), \quad (24)$$

with $\bar{c}_2 = c_2 \frac{(T_{CEP})^{\beta\delta}}{\mu_{B,CEP}}$. We note that this dimensionless treatment allows us to estimate the CEP location which is independent of the scale setting in the truncation scheme. Together with the parameterization of phase transition line, we have

$$T_{CEP} = T_c(0) - \kappa \frac{\mu_{B,CEP}^2}{T_c(0)}, \quad (25)$$

the location of the CEP can be then determined after one extracts the c_2 from the numerical results of LYE singularities in QCD. In Fig. 8, we show the extraction of the c_2 from the LYE singularities.

Through the linear fit between $\text{Im}[\mu_B]^{1/(\beta\delta)}$ and T , one can extract the c_2 directly from the slope, and we get $c_2 = 6.38 \text{ GeV}^{1-\beta\delta}$ and $\bar{c}_2 = 0.28$. Now if here we adopt $\beta\delta$ and z_c from Z(2) universality class and the phase transition line curvature $\kappa = 0.016$ and $T_c(0) = 156 \text{ MeV}$, one gets the CEP at:

$$(T_{CEP}, \mu_{B,CEP}) = (118, 606) \text{ MeV}. \quad (26)$$

This indicates that with the \bar{c}_2 extracted in our work together with the up to date knowledge of the phase transition line and the correct scaling behavior, the obtained CEP location is in precise agreement with the up to date results from the functional QCD approaches [13, 14, 15, 16]. Besides, the rescaled c'_2 based on the estimated CEP now becomes $c'_2 = 5.0 \text{ GeV}^{1-\beta\delta}$. It needs also to mention that one may get a much larger c_2 with the current results of LYE singularities from lattice QCD simulations [45, 46, 47]. It is mainly because the current lattice

QCD results are obtained in too high temperature region and has not reached the scaling region as shown in Fig. 8. For the LYE singularities next to the CEP scaling region, the slope is steeper which stands for a large value of c_2 .

5 Analysis on the parameter dependence in the truncation

In this section, we explore the effects of the parameters in the Ansatz of the quark-gluon interaction vertex in Eq. (5) on the properties of the LYE singularities.

In Eq. (5), we note that the parameters β , δ and Λ are tightly constrained from the running of the quark-gluon vertex function $\Gamma(k^2)$ in (5) at large momentum scale. Specifically, β and δ the anomalous dimensions of the vertex, along with Λ which is related to the QCD scale parameter. The remaining parameters d_1 and d_2 are phenomenological. In previous sections, their values are taken as the parameter set for (2+1)-flavour QCD, which can well describe the meson spectrum. This parameter set will be denoted as set (I) in the following discussion. We then move on to investigate the effect of changing d_1 and d_2 on the results, with the cases of (d_1, d_2) considered in Fig. 2. The obtained variation behavior of some of the characteristic quantities with respect to the d_1 and d_2 are listed in Table 2.

Firstly, we consider the case of changing d_1 together with d_2 , while keeping the obtained vacuum quark mass at zero momentum $M_q(0)$ unchanged (II). With such a setup, we found that the obtained chiral phase transition temperature at zero chemical potential $T_c(0)$ and the location of CEP are very close to the ones obtained from the set (I), see in Table 2. Therefore, the sets (I) and (II) provide explicitly an error estimate on the infrared behaviour of the vertex in (2+1)-flavour QCD. Secondly, we found that the d_2 affects the results less significantly than the d_1 , since the d_2 stands for the running behaviour of the interaction vertex, while d_1 reflects on the vertex strength directly. Therefore, we investigate several d_1 values while keeping d_2 unchanged to test the robustness of the CEP scaling, which is referred to as sets (III) and (IV) in Table 2.

Comparing the results for sets (I)-(IV), it can be found that different d_1 and d_2 parameters yield almost the same critical exponents:

$$\beta\delta \approx 1.37 \pm 0.01, \quad (27)$$

with less than 2% error, implying that the observed CEP scaling of the LYE singularities is a robust property. Moreover, it is clear by comparing the results in the sets (I) and (II) that with the same quark mass $M_q(0)$ obtained, the chiral phase transition line as well as the location of the LYE singularities and their scaling parameters c_2 and \bar{c}_2 are independent to the choice of parameters. We also show that the location of the extracted CEP according to the Z(2) universality class (see the above Sec. 4) is also unchanged from set (I) to set (II).

Table 2. Analysis on the parameter dependence d_1 and d_2 for the chiral phase transition, and the properties of the Lee-Yang edge singularities.

set	(d_1, d_2) GeV ²	$M_q(0)$ GeV	$T_c(0)$ MeV	$(T_{CEP}, \mu_{B,CEP})$ MeV	$\beta\delta$	c_2 GeV ^{1-$\beta\delta$}	\bar{c}_2	$(T'_{CEP}, \mu'_{B,CEP})$ MeV
(I)	(6.8,0.5)	0.36	155.7	(83,723)	1.38	6.38	0.28	(118,606)
(II)	(7.2,0.57)	0.36	155.8	(83,741)	1.36	6.41	0.30	(119,602)
(III)	(7.2,0.5)	0.40	168	(99,708)	1.38	6.8	0.39	(122,578)
(IV)	(8.0,0.5)	0.47	195	(130,642)	1.36	7.1	0.70	(139,540)

On the other hand, by changing the d_1 with the d_2 being maintained constant, the parameter set deviates from the ones for the (2+1)-flavour QCD, which is demonstrated in the change of the chiral phase transition line, i.e. $T_c(0)$ and the CEP location. The scaling parameters c_2 and \bar{c}_2 will also change: generally speaking, they become larger as d_1 increases, or as d_2 decreases. We emphasise, however, that the CEP scaling is still observed, with a similar trend of the LYE singularities at small $\text{Im}\mu_B$. The CEP scaling found here is robust against the choices of parameters.

6 Summary

We calculate the quark gap equation at complex chemical potential with physical quark mass via the Dyson-Schwinger equation approach of QCD. We firstly check the analytic continuity of the phase transition line from imaginary to real chemical potential, which is required in the lattice QCD simulations. Our result shows that the curvature of the chiral phase transition line extracted from the imaginary chemical potential is consistent with that from the real chemical potential.

Moreover, we study the Lee-Yang edge singularities which have been shown to be related to the phase structure at the real chemical potential. We compute the location of the Lee-Yang edge singularities in the complex μ_B plane at different temperatures. Our result manifests that, at the temperature where there is a crossover at the real chemical potential, the Lee-Yang edge singularity is located at the complex plane of the chemical potential with an imaginary part. The absolute value of the imaginary part becomes smaller as the temperature decreases, and finally vanishes at the critical end point temperature.

We then take the Padé polynomials to see whether it is possible to extrapolate the CEP location with the limited range of the Lee-Yang edge singularities. Our result indicates that additional information at high μ_B , especially beyond the range of current best lattice QCD expansions, is required from the theoretical approaches for a precise determination of the CEP.

We further check the scaling behavior of the trajectory of Lee-Yang edge singularities. We compute the radius of the convergence and find that it changes for different temperatures. The value of the convergence radius is also found to be inconsistent with any scaling value for either 3D $O(N)$ or mean field universality class. However, it is found that the LYE singularities follows the CEP scaling

as the Z(2) universality class. Such a scaling behaviour is further confirmed by changing the phenomenological parameters d_1 and d_2 in the truncation scheme. Therefore, one may take the Ising model to study the CEP of QCD. Here we implement a mapping of the QCD order parameters with Ising parameterization, and shows that after extracting c_2 from the current data of the LYE singularities location together with the curvature of the phase transition line, one may extract the location of the CEP with the information of Ising universality class.

For a high temperature, the real part of the Lee-Yang edge singularities becomes smaller and the imaginary part increases which is consistent with the perturbative analysis. The imaginary part is expected to be saturated at $\text{Im}\mu_B = 3\pi T$ which requires a careful scan for a wide range of the complex chemical potential. This may also reveal the periodicity of the thermodynamic quantities which represents the $Z(N_c)$ symmetry and potentially the deconfinement. The related investigation is under progress.

7 Acknowledgements

YL and FG thank the other members of the fQCD collaboration [52] for fruitful discussions. This work is supported by the National Natural Science Foundation of China under Grants No. 12247107, No. 12175007. FG is also supported by the National Science Foundation of China under Grants No. 12305134.

References

1. Aarts, G., *et al.*: Phase Transitions in Particle Physics: Results and Perspectives from Lattice Quantum Chromo-Dynamics. *Prog. Part. Nucl. Phys.* **133**, 104070 (2023) <https://doi.org/10.1016/j.ppnp.2023.104070> arXiv:2301.04382 [hep-lat]
2. Hippert, M., Grefa, J., Manning, T.A., Noronha, J., Noronha-Hostler, J., Portillo Vazquez, I., Ratti, C., Rougemont, R., Trujillo, M.: Bayesian location of the QCD critical point from a holographic perspective (2023) arXiv:2309.00579 [nucl-th]
3. Huang, M., Zhuang, P.: QCD Matter and Phase Transitions under Extreme Conditions. *Symmetry* **15**(2), 541 (2023) <https://doi.org/10.3390/sym15020541>

4. Fu, W.-j.: QCD at finite temperature and density within the fRG approach: an overview. *Commun. Theor. Phys.* **74**(9), 097304 (2022) <https://doi.org/10.1088/1572-9494/ac86be> arXiv:2205.00468 [hep-ph]
5. Lovato, A., et al.: Long Range Plan: Dense matter theory for heavy-ion collisions and neutron stars (2022) arXiv:2211.02224 [nucl-th]
6. Adamczewski-Musch, J., *et al.*: Probing dense baryon-rich matter with virtual photons. *Nature Phys.* **15**(10), 1040–1045 (2019) <https://doi.org/10.1038/s41567-019-0583-8>
7. Fischer, C.S.: QCD at finite temperature and chemical potential from Dyson–Schwinger equations. *Prog. Part. Nucl. Phys.* **105**, 1–60 (2019) <https://doi.org/10.1016/j.pnpnp.2019.01.002> arXiv:1810.12938 [hep-ph]
8. Luo, X., Xu, N.: Search for the QCD Critical Point with Fluctuations of Conserved Quantities in Relativistic Heavy-Ion Collisions at RHIC : An Overview. *Nucl. Sci. Tech.* **28**(8), 112 (2017) <https://doi.org/10.1007/s41365-017-0257-0> arXiv:1701.02105 [nucl-ex]
9. Braun-Munzinger, P., Koch, V., Schäfer, T., Stachel, J.: Properties of hot and dense matter from relativistic heavy ion collisions. *Phys. Rept.* **621**, 76–126 (2016) <https://doi.org/10.1016/j.physrep.2015.12.003> arXiv:1510.00442 [nucl-th]
10. Schaefer, B.-J., Wagner, M.: On the QCD phase structure from effective models. *Prog. Part. Nucl. Phys.* **62**, 381 (2009) <https://doi.org/10.1016/j.pnpnp.2008.12.009> arXiv:0812.2855 [hep-ph]
11. Borsanyi, S., Fodor, Z., Guenther, J.N., Kara, R., Katz, S.D., Parotto, P., Pasztor, A., Ratti, C., Szabo, K.K.: QCD Crossover at Finite Chemical Potential from Lattice Simulations. *Phys. Rev. Lett.* **125**(5), 052001 (2020) <https://doi.org/10.1103/PhysRevLett.125.052001> arXiv:2002.02821 [hep-lat]
12. Bazavov, A., *et al.*: Chiral crossover in QCD at zero and non-zero chemical potentials. *Phys. Lett. B* **795**, 15–21 (2019) <https://doi.org/10.1016/j.physletb.2019.05.013> arXiv:1812.08235 [hep-lat]
13. Gao, F., Pawłowski, J.M.: Chiral phase structure and critical end point in QCD. *Phys. Lett. B* **820**, 136584 (2021) <https://doi.org/10.1016/j.physletb.2021.136584> arXiv:2010.13705 [hep-ph]
14. Gunkel, P.J., Fischer, C.S.: Locating the critical endpoint of QCD: Mesonic backcoupling effects. *Phys. Rev. D* **104**(5), 054022 (2021) <https://doi.org/10.1103/PhysRevD.104.054022> arXiv:2106.08356 [hep-ph]
15. Gao, F., Pawłowski, J.M.: QCD phase structure from functional methods. *Phys. Rev. D* **102**(3), 034027 (2020) <https://doi.org/10.1103/PhysRevD.102.034027> arXiv:2002.07500 [hep-ph]
16. Fu, W.-j., Pawłowski, J.M., Rennecke, F.: QCD phase structure at finite temperature and density. *Phys. Rev. D* **101**(5), 054032 (2020) <https://doi.org/10.1103/PhysRevD.101.054032> arXiv:1909.02991 [hep-ph]
17. Cai, R.-G., He, S., Li, L., Wang, Y.-X.: Probing QCD critical point and induced gravitational wave by black hole physics. *Phys. Rev. D* **106**(12), 121902 (2022) <https://doi.org/10.1103/PhysRevD.106.L121902> arXiv:2201.02004 [hep-th]
18. Yang, C.-N., Lee, T.D.: Statistical theory of equations of state and phase transitions. 1. Theory of condensation. *Phys. Rev.* **87**, 404–409 (1952) <https://doi.org/10.1103/PhysRev.87.404>
19. Lee, T.D., Yang, C.-N.: Statistical theory of equations of state and phase transitions. 2. Lattice gas and Ising model. *Phys. Rev.* **87**, 410–419 (1952) <https://doi.org/10.1103/PhysRev.87.410>
20. Clarke, D.A., Zambello, K., Dimopoulos, P., Di Renzo, F., Goswami, J., Nicotra, G., Schmidt, C., Singh, S.: Determination of Lee-Yang edge singularities in QCD by rational approximations. *PoS LATTICE2022*, 164 (2023) <https://doi.org/10.22323/1.430.0164> arXiv:2301.03952 [hep-lat]
21. Schmidt, C., Clarke, D.A., Nicotra, G., Di Renzo, F., Dimopoulos, P., Singh, S., Goswami, J., Zambello, K.: Detecting Critical Points from the Lee–Yang Edge Singularities in Lattice QCD. *Acta Phys. Polon. Supp.* **16**(1), 1–52 (2023) <https://doi.org/10.5506/APhysPolBSupp.16.1-A52> arXiv:2209.04345 [hep-lat]
22. Singh, S., Dimopoulos, P., Dini, L., Di Renzo, F., Goswami, J., Nicotra, G., Schmidt, C., Zambello, K., Ziesche, F.: Lee-Yang edge singularities in lattice QCD : A systematic study of singularities in the complex μB plane using rational approximations. *PoS LATTICE2021*, 544 (2022) <https://doi.org/10.22323/1.396.0544> arXiv:2111.06241 [hep-lat]
23. Roberge, A., Weiss, N.: Gauge Theories With Imaginary Chemical Potential and the Phases of QCD. *Nucl. Phys. B* **275**, 734–745 (1986) [https://doi.org/10.1016/0550-3213\(86\)90582-1](https://doi.org/10.1016/0550-3213(86)90582-1)
24. Fischer, C.S., Luecker, J., Pawłowski, J.M.: Phase structure of QCD for heavy quarks. *Phys. Rev. D* **91**(1), 014024 (2015) <https://doi.org/10.1103/PhysRevD.91.014024> arXiv:1409.8462 [hep-ph]
25. Fischer, C.S.: Deconfinement phase transition and the quark condensate. *Phys. Rev. Lett.* **103**, 052003 (2009) <https://doi.org/10.1103/PhysRevLett.103.052003> arXiv:0904.2700 [hep-ph]
26. Fischer, C.S., Luecker, J., Mueller, J.A.: Chiral and deconfinement phase transitions of two-flavour QCD at finite temperature and chemical potential. *Phys. Lett. B* **702**, 438–441 (2011) <https://doi.org/10.1016/j.physletb.2011.07.039> arXiv:1104.1564 [hep-ph]
27. Alkofer, R., Smekal, L.: The Infrared behavior of QCD Green’s functions: Confinement dynamical symmetry breaking, and hadrons as relativistic bound states. *Phys. Rept.* **353**, 281 (2001) [https://doi.org/10.1016/S0370-1573\(01\)00010-2](https://doi.org/10.1016/S0370-1573(01)00010-2) arXiv:hep-ph/0007355

28. Roberts, C.D.: Hadron Properties and Dyson-Schwinger Equations. *Prog. Part. Nucl. Phys.* **61**, 50–65 (2008) <https://doi.org/10.1016/j.ppnp.2007.12.034> arXiv:0712.0633 [nucl-th]
29. Fischer, C.S., Luecker, J., Welzbacher, C.A.: Phase structure of three and four flavor QCD. *Phys. Rev. D* **90**(3), 034022 (2014) <https://doi.org/10.1103/PhysRevD.90.034022> arXiv:1405.4762 [hep-ph]
30. Gao, F., Papavassiliou, J., Pawłowski, J.M.: Fully coupled functional equations for the quark sector of QCD. *Phys. Rev. D* **103**(9), 094013 (2021) <https://doi.org/10.1103/PhysRevD.103.094013> arXiv:2102.13053 [hep-ph]
31. Vija, H., Thoma, M.H.: Braaten-Pisarski method at finite chemical potential. *Phys. Lett. B* **342**, 212–218 (1995) [https://doi.org/10.1016/0370-2693\(94\)01378-P](https://doi.org/10.1016/0370-2693(94)01378-P) arXiv:hep-ph/9409246
32. Haque, N., Mustafa, M.G., Strickland, M.: Two-loop hard thermal loop pressure at finite temperature and chemical potential. *Phys. Rev. D* **87**(10), 105007 (2013) <https://doi.org/10.1103/PhysRevD.87.105007> arXiv:1212.1797 [hep-ph]
33. Bowman, P.O., Heller, U.M., Leinweber, D.B., Parappilly, M.B., Williams, A.G., Zhang, J.-b.: Unquenched quark propagator in Landau gauge. *Phys. Rev. D* **71**, 054507 (2005) <https://doi.org/10.1103/PhysRevD.71.054507> arXiv:hep-lat/0501019
34. Gao, F., Liu, Y.-x.: QCD phase transitions via a refined truncation of Dyson-Schwinger equations. *Phys. Rev. D* **94**(7), 076009 (2016) <https://doi.org/10.1103/PhysRevD.94.076009> arXiv:1607.01675 [hep-ph]
35. Lu, Y., Gao, F., Liu, Y.-X., Pawłowski, J.M.: QCD equation of state and thermodynamic observables from computationally minimal Dyson-Schwinger Equations (2023) arXiv:2310.18383 [hep-ph]
36. Bernhardt, J., Fischer, C.S.: From imaginary to real chemical potential QCD with functional methods. *Eur. Phys. J. A* **59**(8), 181 (2023) <https://doi.org/10.1140/epja/s10050-023-01098-1> arXiv:2305.01434 [hep-ph]
37. Basar, G.: Universality, Lee-Yang Singularities, and Series Expansions. *Phys. Rev. Lett.* **127**(17), 171603 (2021) <https://doi.org/10.1103/PhysRevLett.127.171603> arXiv:2105.08080 [hep-th]
38. Zinn-Justin, J.: Quantum Field Theory and Critical Phenomena. International Series of Monographs on Physics, vol. 77. Oxford University Press, ??? (2021)
39. Connelly, A., Johnson, G., Rennecke, F., Skokov, V.: Universal Location of the Yang-Lee Edge Singularity in $O(N)$ Theories. *Phys. Rev. Lett.* **125**(19), 191602 (2020) <https://doi.org/10.1103/PhysRevLett.125.191602> arXiv:2006.12541 [cond-mat.stat-mech]
40. Johnson, G., Rennecke, F., Skokov, V.V.: Universal location of Yang-Lee edge singularity in classic $O(N)$ universality classes. *Phys. Rev. D* **107**(11), 116013 (2023) <https://doi.org/10.1103/PhysRevD.107.116013> arXiv:2211.00710 [hep-ph]
41. Rennecke, F., Skokov, V.V.: Universal location of Yang–Lee edge singularity for a one-component field theory in $1 \leq d \leq 4$. *Annals Phys.* **444**, 169010 (2022) <https://doi.org/10.1016/j.aop.2022.169010> arXiv:2203.16651 [hep-ph]
42. Kos, F., Poland, D., Simmons-Duffin, D., Vichi, A.: Precision Islands in the Ising and $O(N)$ Models. *JHEP* **08**, 036 (2016) [https://doi.org/10.1007/JHEP08\(2016\)036](https://doi.org/10.1007/JHEP08(2016)036) arXiv:1603.04436 [hep-th]
43. Kaczmarek, O., Karsch, F., Laermann, E., Miao, C., Mukherjee, S., Petreczky, P., Schmidt, C., Soeldner, W., Unger, W.: Phase boundary for the chiral transition in (2+1)-flavor QCD at small values of the chemical potential. *Phys. Rev. D* **83**, 014504 (2011) <https://doi.org/10.1103/PhysRevD.83.014504> arXiv:1011.3130 [hep-lat]
44. Mukherjee, S., Skokov, V.: Universality driven analytic structure of the QCD crossover: radius of convergence in the baryon chemical potential. *Phys. Rev. D* **103**(7), 071501 (2021) <https://doi.org/10.1103/PhysRevD.103.L071501> arXiv:1909.04639 [hep-ph]
45. Goswami, J., Clarke, D.A., Dimopoulos, P., Di Renzo, F., Schmidt, C., Singh, S., Zambello, K.: Exploring the Critical Points in QCD with Multi-Point Padé and Machine Learning Techniques in (2+1)-flavor QCD (2024) arXiv:2401.05651 [hep-lat]
46. Dimopoulos, P., Dini, L., Di Renzo, F., Goswami, J., Nicotra, G., Schmidt, C., Singh, S., Zambello, K., Ziesché, F.: Contribution to understanding the phase structure of strong interaction matter: Lee-yang edge singularities from lattice qcd. *Phys. Rev. D* **105**, 034513 (2022) <https://doi.org/10.1103/PhysRevD.105.034513>
47. Bollweg, D., Goswami, J., Kaczmarek, O., Karsch, F., Mukherjee, S., Petreczky, P., Schmidt, C., Scior, P.: Taylor expansions and Padé approximants for cumulants of conserved charge fluctuations at nonvanishing chemical potentials. *Phys. Rev. D* **105**(7), 074511 (2022) <https://doi.org/10.1103/PhysRevD.105.074511> arXiv:2202.09184 [hep-lat]
48. Stephanov, M.A.: Qcd critical point and complex chemical potential singularities. *Phys. Rev. D* **73**, 094508 (2006) <https://doi.org/10.1103/PhysRevD.73.094508>
49. Lu, Y., Gao, F., Fu, B.-C., Song, H.-C., Liu, Y.-X.: Constructing the Equation of State of QCD in a functional QCD based scheme (2023) arXiv:2310.16345 [hep-ph]
50. Parotto, P., Bluhm, M., Mroczek, D., Nahrgang, M., Noronha-Hostler, J., Rajagopal, K., Ratti, C., Schäfer, T., Stephanov, M.: Qcd equation of state matched to lattice data and exhibiting a critical point singularity. *Phys. Rev. C* **101**, 034901 (2020) <https://doi.org/10.1103/PhysRevC.101.034901>
51. Rehr, J.J., Mermin, N.D.: Revised scaling equation of state at the liquid-vapor critical point. *Phys. Rev. A* **8**, 472–480 (1973) <https://doi.org/10.1103/PhysRevA.8.472>
52. Braun, J., Chen, Y.-r., Fu, W.-j., Gao, F., Geissel, A.,

Horak, J., Huang, C., Ihssen, F., Lu, Y., Pawłowski, J.M., Rennecke, F., Sattler, F., Schallmo, B., Stoll, J., Tan, Y.-y., Töpfel, S., Turnwald, J., Wen, R., Wessely, J., Wink, N., Yin, S., Zorbach, N.: fQCD collaboration (2023)